Polytope-based Aggregation Method for User-side Flexible Energy Resources to Improve Flexibility of Active Distribution Networks

Jing Wang, *Student Member*, *IEEE*, Muyang Liu, *Member*, *IEEE*, Junru Chen, *Member*, *IEEE*, Haochen Hua, *Member*, *IEEE*, Lijiao Gong, *Senior Member*, *IEEE*, and Weiqing Wang

***Abstract*—Improving the flexibility of active distribution networks (ADNs) enhances the reliability and economic performance of regional power systems. Common user-side flexible energy resources (FERs), which are numerous but individually limited in capacity, can be aggregated to participate in ADN operations. To accurately and efficiently aggregate heterogeneous user-side FERs, this paper proposes a novel polytope-based aggregation method to construct the aggregated feasible region, which is integrated into a coordinated operation model for ADNs. The proposed method employs an inner approximation using affine transformation to better capture the feasible regions of individual FERs. In addition, a distributionally robust chance-constrained (DRCC) model is integrated to address parameter uncertainties in FERs, and a rolling mechanism is applied to intraday operations for the rolling update of the aggregated feasible region. Finally, a case study of a specific ADN in Northwest China validates the effectiveness of the proposed method and the corresponding improvement in flexibility. The results indicate that the proposed coordinated operation model effectively improves the flexibility of ADNs, and the proposed method reduces the computational burden without compromising economic benefits.**

***Index Terms*—Flexible energy resource (FER), active distribution network (ADN), feasible region, flexibility, affine transformation, distributionally robust chance-constrained (DRCC) model.**

Manuscript received: August 21, 2025; revised: November 25, 2025; accepted: January 23, 2026. Date of CrossCheck: January 23, 2026. Date of online publication: April 2, 2026.

This work was supported by Department of Science and Technology of Xinjiang Uygur Autonomous Region (No. 2025E01034), Science and Technology Bureau of Xinjiang Production and Construction Corps (No. 2024AA004), and Autonomous Region Graduate Research and Innovation Program (No. XJ2024G046).

J. Wang, M. Liu, J. Chen (corresponding author), and W. Wang are with the School of Electrical Engineering, Xinjiang University, Urumqi, China (e-mail: wangjing@stu. xju. edu. cn; muyang. liu@xju. edu. cn; junru. chen@xju. edu. cn; wwq59@xju.edu.cn).

H. Hua is with the College of Energy and Electrical Engineering, Hohai University, Nanjing, China (e-mail: huahc16@tsinghua.org.cn).

L. Gong is with the School of Electrical Engineering, Shihezi University, Shihezi, China (e-mail: glj_mac@shzu.edu.cn).

DOI: 10.35833/MPCE.2025.000776

I. Introduction

THE rapid development of renewable energy is driving the transformation of the global energy structure. Certain passive distribution networks are transitioning to active distribution networks (ADNs) with integrated distributed energy resources (DERs) such as wind generation (WG) and photovoltaic (PV) cells [1]. In this context, the stochastic nature of DERs, together with the variability of modern load, increases the uncertainty within ADNs. This degrades the reliability of power supply and therefore increases the demand for flexibility, that is, the ability to manage the variations and uncertainty in the power system [2]. At the same time, the new devices that can behave as controllable loads in ADNs, including user-side energy storages (ESs), electric vehicles (EVs), and thermostatically controlled loads (TCLs), provide the potential to improve the flexibility of ADNs by allowing demand regulation in response to the temporal distribution of DERs. These devices are thus referred to as user-side flexible energy resources (FERs) [3]. However, the large quantity, wide geographical distribution, and heterogeneous operational characteristics of FERs make the scheduling of individual resources technically impractical, as it would impose costs in terms of communication and computation, while being incompatible with the flexibility demand of ADNs. Therefore, the aggregation of FERs is essential for the control and operation of ADNs. The aggregation of FERs is defined as the calculation of feasible regions for power and energy, taking into account various parameters and operational constraints [4]. With the increasing number of FERs, aggregation becomes a high-dimensional nonlinear problem [5], which may eventually become unsolvable due to the unaffordable computational burden. Furthermore, certain FERs such as EVs and TCLs exhibit different operational characteristics and regulatory capability that are influenced by environmental factors and human behavior [6]. For modern ADNs, challenges remain in the accurate aggregation of various FERs, and the utilization of the capability of FERs to improve the flexibility of the entire distribution network.

In response to these challenges, the operational and control characteristics of FERs have been extensively studied. The virtual battery (VB) model is a widely used modeling method for describing the regulation capability of FERs [7]-[9]. This model is a scalar linear system that simulates simplified battery dynamics, defined by parameters such as charging/discharging power limits, energy capacity, and self-discharge rates. For example, [10] aggregated battery-type FERs into a VB and proposed a boundary contraction method using a high-dimensional polytope, specifically for parameter estimation within the VB model. However, existing VB models tend to be conservative when characterizing aggregated feasible regions, particularly for large groups of resources with heterogeneous parameters. Therefore, describing the feasible region of a single resource as a convex polytope in half-space representation (H-representation) provides a starting point for capturing the entire feasible region of a FER cluster [11]. The Minkowski sum, which performs addition operations in Euclidean space [12], can then be used to construct the aggregation methods for each cluster.

In reality, the exact aggregated feasible region is equivalent to the Minkowski sum of the feasible regions of all FERs [13]. However, performing the Minkowski sum operation on polytopes using H-representation is generally non-deterministic polynomial-time hard (NP-hard) [14]. To reduce model complexity, researchers have developed several effective approximation methods. These methods are classified into inner approximation and outer approximation, providing subsets and supersets of the aggregated feasible region, respectively [15]. A major limitation of outer approximation methods is that they may include infeasible solutions, which fail to satisfy scheduling constraints after the FERs are disaggregated [16]. Inner approximation methods can avoid this limitation by introducing conservatism when approximating the aggregated feasible region, but this may lead to the shrinkage of the aggregated feasible region [17]. To address this conservatism, geometric constructs such as zonotopes [18] and homothets [19] of convex polytopes have been adopted, resulting in more accurate inner approximation feasible regions based on convex optimization. Although these methods can approximate the true Minkowski sum using numerous hyperrectangles, their scalability in large-scale systems is restricted by the rapidly growing computational burden. Therefore, for addressing the aggregation of large-scale FERs, how to decrease computational burden without neglecting individual characteristics of each resource remains an open question.

Most existing studies have applied aggregation methods to real-world power system scheduling, reporting the aggregated feasible region and leaving the decision-making for power scheduling to upper-level system operators with the goal of improving economic efficiency [20]. However, factors such as residents' living behavior, travel patterns, and ambient temperature significantly affect the electricity consumption patterns of FERs [21]. Such uncertain parameters directly influence the accuracy of the aggregated feasible region, resulting in infeasible scheduling. Although stochastic optimization [22] and robust optimization [23] have been employed to address these problems, both methods present notable limitations for feasible region aggregation. Stochastic optimization depends on the generation of a large number of scenarios, leading to substantial computational burdens, whereas robust optimization targets low-probability worst-case scenarios, producing overly conservative models [16]. In response, distributionally robust chance-constrained (DRCC) models have been proposed to address uncertainty in aggregation, as they are more tractable and deliver superior out-of-sample performance [24], [25]. Nevertheless, as the scale of FERs grows, effectively incorporating DRCC into aggregation methods for optimal operation of modern ADNs—while balancing model accuracy, computational efficiency, and scheduling feasibility—remains a critical technical challenge.

In response to the research problems described above, this paper proposes a polytope-based aggregation method and a coordinated operation model for large-scale heterogeneous user-side FERs to improve the flexibility of ADNs. The main contributions of this paper are summarized as follows:

1) A polytope-based aggregation method using inner approximation is proposed. Utilizing full-dimensional affine transformations, the proposed method updates the scaling factor of linear transformation matrices to capture the heterogeneity of individual FERs, thereby reducing the conservatism of the aggregated feasible region compared to existing methods.

2) A DRCC model and an intraday rolling mechanism are incorporated into the proposed method. This integration enables dynamic adjustment of the aggregated feasible region in response to uncertainties, thereby enhancing operational adaptability to real-time conditions and providing a robust coordinated operation model for ADN.

3) A coordinated operation model for improving the flexibility of ADNs is established by using the proposed method. A case study demonstrates that this model achieves an effective trade-off between computational tractability and aggregation accuracy, substantially improves system flexibility, reduces operation costs, and outperforms conventional methods in overall performance and scheduling feasibility.

The remainder of this paper is organized as follows. Section II establishes the feasible regions for individual FERs. Section III describes the proposed polytope-based aggregation method for heterogeneous user-side FERs. Section IV describes the proposed coordinated operation model for flexibility improvement. Section V presents a case study. Section VI provides the conclusions.

II. Feasible Regions for Individual FERs

User-side FERs including ESs, EVs and TCLs, provide grid services through contracts with the distribution system operator (DSO). Given their distinct and interrelated operational constraints, a unified mathematical representation of their feasible region is crucial for efficient optimization. This section discusses the feasible region for individual FERs, and employs a unified H-representation to handle heterogeneous constraint characteristics, thereby establishing a mathematically rigorous foundation for the aggregation and coordination of large-scale heterogeneous user-side FERs in subsequent subsections.

A. ESs

ESs can provide bidirectional regulation capability. The operational characteristics and constraints for ES i are formulated as:

$$0 \le P_{ES,i,t}^{dis} \le P_{ES,i}^{dis,\max} \tag{1}$$

$$0 \le P_{ES,i,t}^{ch} \le P_{ES,i}^{ch,\max} \tag{2}$$

$$\eta_{ES}\sum_{t=1}^{T} P_{ES,i,t}^{ch}\Delta t = \frac{1}{\eta_{ES}}\sum_{t=1}^{T} P_{ES,i,t}^{dis}\Delta t \tag{3}$$

$$E_{ES,i,t} = E_{ES,i,t-1} + \eta_{ES} P_{ES,i,t}^{ch}\Delta t - \frac{1}{\eta_{ES}} P_{ES,i,t}^{dis}\Delta t \tag{4}$$

$$E_{ES,i}^{\min} \le E_{ES,i,t} \le E_{ES,i}^{\max} \tag{5}$$

where $P_{ES,i,t}^{ch}$ and $P_{ES,i,t}^{dis}$ are the charging and discharging power of ES i at time t, respectively; $E_{ES,i,t}$ is the energy state of ES i at time t; $P_{ES,i}^{ch,\max}$ and $P_{ES,i}^{dis,\max}$ are the maximum charging and discharging power of ES i, respectively; $E_{ES,i}^{\max}$ and $E_{ES,i}^{\min}$ are the maximum and minimum energy capacities of ES i, respectively; η_{ES} is the charging/discharging efficiency of ES; Δt is the time interval; and T is the total number of time periods. Following [24], we omit the complementary constraints to prevent simultaneous charging and discharging, thereby significantly improving the computational tractability of the aggregation problems.

The flexibility regulation ranges are formulated as:

$$0 \le \underline{E}_{ES,i,t} \le \min\{(P_{ES,i}^{dis,\max}/\eta_{ES} - P_{ES,i,t}^{dis})\Delta t, E_{ES,i,t} - E_{ES,i}^{\min}\} \tag{6}$$

$$0 \le \bar{E}_{ES,i,t} \le \min\{(\eta_{ES} P_{ES,i}^{ch,\max} - P_{ES,i,t}^{ch})\Delta t, E_{ES,i}^{\max} - E_{ES,i,t}\} \tag{7}$$

where $\bar{E}_{ES,i,t}$ and $\underline{E}_{ES,i,t}$ are the upward and downward energy regulation ranges of ES i at time t, respectively.

The operational constraints of the ES in (1)-(7) collectively form a compact, convex polytope. This feasible region can be equivalently represented in its H-representation, which defines a convex polytope as the bounded intersection of a finite number of closed half-spaces [25]. The H-representation polytope of the ES is expressed as:

$$\mathbb{Z}_{ES,i} = \{\boldsymbol{X}_{ES,i} \in \mathbb{R}^{2T} | \boldsymbol{W}_{ES,i}\boldsymbol{X}_{ES,i} \le \boldsymbol{M}_{ES,i}\} \tag{8}$$

where $\mathbb{Z}_{ES,i}$ is the feasible region of ES i; $\boldsymbol{W}_{ES,i}$ is the matrix encoding the linear constraints; $\boldsymbol{X}_{ES,i}$ is the vector of decision variables representing charging and discharging power of ES i; and $\boldsymbol{M}_{ES,i}$ is the vector of constants representing the upper or lower bounds for each constraint.

B. EVs

EVs can operate as flexible loads in both time and space. With the advancement of vehicle-to-grid (V2G) techniques, their rapid response and ES capabilities can improve system flexibility. The feasible region of each EV depends on a set of parameters [26]. Given the individual-specific parameter Θ_{EV}, EVs are partitioned into K clusters using the K-means method for modeling. The model of EV i in cluster k at time t is formulated as:

$$0 \le P_{EV,k,i,t}^{ch} \le P_{EV,k,i}^{ch,\max} \tag{9}$$

$$0 \le P_{EV,k,i,t}^{dis} \le P_{EV,k,i}^{dis,\max} \tag{10}$$

$$\underline{E}_{EV,k,i,t} \le E_{EV,k,i,t} \le \bar{E}_{EV,k,i,t} \tag{11}$$

$$E_{EV,k,i,t+1} = E_{EV,k,i,t} + \Delta t(\eta_{EV} P_{EV,k,i,t}^{ch} - P_{EV,k,i,t}^{dis}/\eta_{EV}) \tag{12}$$

$$\bar{E}_{EV,k,i,t} = \min\{E_{EV,k,i}^{\max}, E_{EV,k,i,ta} + \eta_{EV} P_{EV,k,i}^{ch,\max}(t - t_{EV,k,i,a})\} \tag{13}$$

$$\begin{aligned}\underline{E}_{EV,k,i,t} = \max\{&E_{EV,k,i}^{\min}, E_{EV,k,i,ta} - P_{EV,k,i}^{dis,\max}(t - t_{EV,k,i,a})/\eta_{EV},\\ &E_{EV,k,i}^{e} - \eta_{EV} P_{EV,k,i}^{ch,\max}(t_{EV,k,i,l} - t)\}\end{aligned} \tag{14}$$

where $P_{EV,k,i,t}^{ch}$ and $P_{EV,k,i,t}^{dis}$ are the charging and discharging power of EV i in cluster k at time t, respectively; $E_{EV,k,i,t}$ is the energy state of EV i in cluster k at time t; $P_{EV,k,i}^{ch,\max}$ and $P_{EV,k,i}^{dis,\max}$ are the maximum charging and discharging power of EV i in cluster k, respectively; $E_{EV,k,i}^{\min}$ and $E_{EV,k,i}^{\max}$ are the minimum and maximum energy capacities of EV i in cluster k, respectively; $\bar{E}_{EV,k,i,t}$ and $\underline{E}_{EV,k,i,t}$ are the upward and downward energy regulation ranges of EV i in cluster k at time t, respectively; $t_{EV,k,i,a}$ and $t_{EV,k,i,l}$ are the arrival and departure time of EV i in cluster k, respectively; $E_{EV,k,i,ta}$ is the initial energy of EV i in cluster k; $E_{EV,k,i}^{e}$ is the desired energy of EV i in cluster k; and η_{EV} is the charging/discharging efficiency of EV.

By combining (9)-(14), the H-representation polytope of the EV is obtained as:

$$\mathbb{Z}_{EV,k,i} = \{\boldsymbol{X}_{EV,k,i} \in \mathbb{R}^{2T} | \boldsymbol{W}_{EV,k,i}\boldsymbol{X}_{EV,k,i} \le \boldsymbol{M}_{EV,k,i}\} \tag{15}$$

where $\mathbb{Z}_{EV,k,i}$ is the feasible region of EV i in cluster k; $\boldsymbol{W}_{EV,k,i}$ and $\boldsymbol{M}_{EV,k,i}$ are the coefficient matrix and vector of EV i in cluster k, respectively; and $\boldsymbol{X}_{EV,k,i}$ is the vector of decision variables representing the charging and discharging power of EV i in cluster k.

The charging and discharging time of EV users is determined by their contracts with the DSO. However, uncertainty remains in $E_{EV,k,i,ta}$ and $E_{EV,k,i}^{e}$.

C. TCLs

Although the operational principles of TCLs differ from those of ESs, their regulation characteristics are similar [27]. Since the regulation capability of a TCL depends on the ambient temperature Υ_{out} and the temperature setpoint Υ_{set}, the K-means method is applied to clustering. To linearize the nonlinear thermal dynamics, the method in [11] is used to derive the power and energy consumption bounds of a TCL operating within its temperature deadband, leading to the following equivalent representation:

$$\underline{P}_{TCL,k,i,t} \le P_{TCL,k,i,t} \le \bar{P}_{TCL,k,i,t} \tag{16}$$

$$\underline{E}_{TCL,k,i,t} \le E_{TCL,k,i,t} \le \bar{E}_{TCL,k,i,t} \tag{17}$$

$$E_{TCL,k,i,t+1} = \varphi E_{TCL,k,i,t} + P_{TCL,k,i,t}\Delta t \tag{18}$$

where $P_{TCL,k,i,t}$ and $E_{TCL,k,i,t}$ are the power and energy of TCL i in cluster k at time t, respectively; $\bar{P}_{TCL,k,i,t}$ and $\underline{P}_{TCL,k,i,t}$ are the upward and downward power regulation ranges of TCL i in cluster k at time t, respectively; $\bar{E}_{TCL,k,i,t}$ and $\underline{E}_{TCL,k,i,t}$ are the upward and downward energy regulation ranges of TCL i in cluster k at time t, respectively; and φ is the coefficient of performance.

The H-representation polytope of the TCL is expressed as:

$$\mathbb{Z}_{TCL,k,i} = \{\boldsymbol{X}_{TCL,k,i} \in \mathbb{R}^{T} | \boldsymbol{W}_{TCL,k,i}\boldsymbol{X}_{TCL,k,i} \le \boldsymbol{M}_{TCL,k,i}\} \tag{19}$$

where $\mathbb{Z}_{TCL,k,i}$ is the feasible region of TCL i in cluster k; $\boldsymbol{W}_{TCL,k,i}$ and $\boldsymbol{M}_{TCL,k,i}$ are the coefficient matrix and vector of

TCL i in cluster k, respectively; and $\boldsymbol{X}_{TCL,k,i}$ is the vector of decision variables of TCL i in cluster k.

Similar to EVs, the flexibility regulation capability of TCLs also depends on $\varUpsilon_{out}$ and $\varUpsilon_{set}$. Therefore, the uncertain parameters $\boldsymbol{\xi}=[E_{EV,k,i,ta}, E^{e}_{EV,k,i}, \varUpsilon_{out}, \varUpsilon_{set}]$ must be continuously updated to ensure effective regulation under varying conditions. The specific effects on dynamic aggregation and coordinated operation are detailed in Section IV.

III. Proposed Polytope-based Aggregation Method for Heterogeneous User-side FERs

In this section, building on the unified H-representation of feasible regions from Section II, we propose a polytope-based aggregation method based on a full-dimensional affine transformation. To address the uncertain parameters $\boldsymbol{\xi}$ that affect the feasible regions of FERs, a DRCC model is incorporated. The proposed method aims to derive the aggregated feasible region for clusters of heterogeneous user-side FERs, which can be directly utilized by the DSO for coordinated operation. It consists of four steps, as shown in Fig. 1.

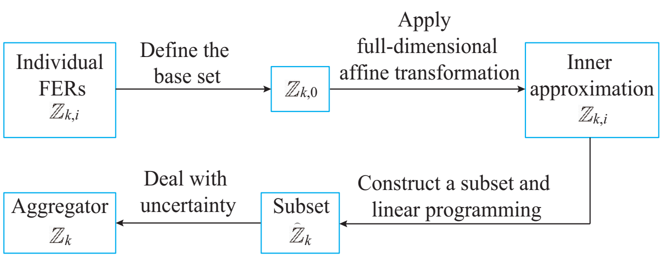

Fig. 1. Schematic diagram of proposed method.

1) Define the base set

As discussed in Section II, the K-means method enables a more distinct characterization of the flexibility offered by FERs with heterogeneous parameters. Building on (8), (15), and (19), the model of FER i in cluster k is formulated as a polytope using the H-representation of linear inequality constraints:

$$\mathbb{Z}_{k,i}=\{\boldsymbol{X}_{k,i}\in\mathbb{R}^{2T} | \boldsymbol{W}_{k,i}\boldsymbol{X}_{k,i}\leq \boldsymbol{M}_{k,i}\} \tag{20}$$

where $\mathbb{Z}_{k,i}$ is the feasible region of FER i in cluster k; $\boldsymbol{W}_{k,i}$ and $\boldsymbol{M}_{k,i}$ are the coefficient matrix and vector of FER i in cluster k, respectively; and $\boldsymbol{X}_{k,i}$ is the vector of decision variables of FER i in cluster k.

The proposed method employs a base set $\mathbb{Z}_{k,0}$ to capture the flexibility structure of FERs within a cluster. Drawing on the averaging method [17], the base set can balance representativeness and computational tractability, reducing complexity for subsequent affine transformations while retaining core flexibility characteristics.

$$\mathbb{Z}_{k,0}=\{\boldsymbol{X}_{k,i}\in\mathbb{R}^{2T} | \boldsymbol{W}_{k,0}\boldsymbol{X}_{k,i}\leq \boldsymbol{M}_{k,0}\} \tag{21}$$

where $\boldsymbol{M}_{k,0}$ is the average vector of $\boldsymbol{M}_{k,i}$; and $\boldsymbol{W}_{k,0}$ is the average coefficient matrix of $\boldsymbol{W}_{k,i}$.

2) Apply full-dimensional affine transformation

The exact aggregated feasible region of cluster k can be expressed as the Minkowski sum of the feasible regions $\mathbb{Z}_{k,i}$ of individual FERs:

$$\mathbb{Z}_k=\bigoplus_{i\in\mathcal{N}_k}\mathbb{Z}_{k,i}=\left\{\boldsymbol{X}_k\in\mathbb{R}^{2T} \,\middle|\, \boldsymbol{X}_k=\sum_{i\in\mathcal{N}_k}\boldsymbol{X}_{k,i}, \boldsymbol{X}_{k,i}\in\mathbb{Z}_{k,i}\right\} \tag{22}$$

where $\mathbb{Z}_k$ is the polytope in $\mathbb{R}^{2T}$ aggregated feasible region of cluster k; the symbol $\oplus$ denotes the Minkowski sum operation; $\boldsymbol{X}_k$ is the vector of decision variables of FER in cluster k; and $\mathcal{N}_k$ is the set of FERs in cluster k.

Since computing the Minkowski sum of H-polytopes is NP-hard, we employ full-dimensional affine transformations to map each individual feasible region from $\mathbb{Z}_{k,0}$. Specifically, for FER i in cluster k, its feasible regions $\mathbb{Z}_{k,i}$ can be represented as a full-dimensional affine transformation of the base set $\mathbb{Z}_{k,0}$:

$$\boldsymbol{A}_{k,i}\mathbb{Z}_{k,0}+\boldsymbol{b}_{k,i}\subseteq\mathbb{Z}_{k,i} \tag{23}$$

where $\boldsymbol{A}_{k,i}\in\mathbb{R}^{2T\times 2T}$ is the full-dimensional linear transformation matrix; and $\boldsymbol{b}_{k,i}\in\mathbb{R}^{2T}$ is the translation vector.

By exploiting the linearity property of Minkowski sums under affine transformations, the aggregated feasible region satisfies:

$$\begin{aligned}&(\boldsymbol{A}_{k,1}\mathbb{Z}_{k,0}+\boldsymbol{b}_{k,1})\oplus\ldots\oplus(\boldsymbol{A}_{k,i}\mathbb{Z}_{k,0}+\boldsymbol{b}_{k,i})\oplus\ldots\oplus\\&(\boldsymbol{A}_{k,\mathcal{N}_k}\mathbb{Z}_{k,0}+\boldsymbol{b}_{k,\mathcal{N}_k})=\sum_{i=\mathcal{N}_k}\boldsymbol{A}_{k,i}\mathbb{Z}_{k,0}+\sum_{i=\mathcal{N}_k}\boldsymbol{b}_{k,i}\subseteq\mathbb{Z}_k\end{aligned} \tag{24}$$

3) Construct a subset and linear programming

Directly determining $\boldsymbol{A}_{k,i}$ and $\boldsymbol{b}_{k,i}$ is computationally intractable due to the non-convex optimization problem in high-dimensional spaces. Consequently, we seek an inner approximation subset $\hat{\mathbb{Z}}_k$ of $\mathbb{Z}_k$, defined as an affine transformation of $\mathbb{Z}_{k,0}$:

$$\boldsymbol{\gamma}_k\mathbb{Z}_{k,0}+\boldsymbol{\varphi}_k\subseteq\hat{\mathbb{Z}}_k\subseteq\mathbb{Z}_k \tag{25}$$

where $\boldsymbol{\gamma}_k\in\mathbb{R}^{2T\times 2T}$ and $\boldsymbol{\varphi}_k\in\mathbb{R}^{2T}$ are the linear transformation matrix and translation vector of the subset in cluster k, respectively.

To achieve a tight approximation of $\mathbb{Z}_k$ by $\hat{\mathbb{Z}}_k$, we adopt the objective of maximizing the volume of $\hat{\mathbb{Z}}_k$. Following [24], which employs the matrix of auxiliary variables $\boldsymbol{G}_{k,i}$ and the polytope inclusion theorem, this leads to the following optimization problem:

$$\begin{cases}\max\limits_{\boldsymbol{\gamma}_k,\boldsymbol{\varphi}_k} Tr(\boldsymbol{\gamma}_k)\\ \text{s.t.}\;\; \boldsymbol{G}_{k,i}\boldsymbol{W}_{k,i}=\boldsymbol{W}_{k,i}\boldsymbol{A}_{k,i}\\ \qquad \boldsymbol{G}_{k,i}\boldsymbol{M}_{k,0}\leq\boldsymbol{M}_{k,i}-\boldsymbol{W}_{k,i}\boldsymbol{b}_{k,i}\end{cases} \tag{26}$$

where $Tr(\cdot)$ is the trace of $\boldsymbol{\gamma}_k$.

To preserve individual characteristics, this study derives the core conditions $\boldsymbol{\gamma}_k=\sum_{i\in\mathcal{N}_k}\boldsymbol{A}_{k,i}$ and $\boldsymbol{\varphi}_k=\sum_{i\in\mathcal{N}_k}\boldsymbol{b}_{k,i}$ to ensure the inclusion relationship between the inner approximation and the exact aggregated feasible region, based on the properties of the Minkowski sums of affine transformations for individual FERs and the aggregated feasible region.

4) Deal with uncertainty

The uncertain parameters $\boldsymbol{\xi}$ in $\boldsymbol{M}_{k,i}$ affect the aggregated feasible region. To address this, the proposed method focuses on parameter uncertainties and employs a DRCC model, which is widely adopted for its independence from exact probability distributions and its characterization of uncertainty via ambiguity sets [28]. The ambiguity set of $\mathcal{D}_i$ for $\boldsymbol{M}_{k,i}$ with uncertain parameters $\boldsymbol{\xi}$ is given as:

$$\mathcal{D}_i=\{\mathbb{E}[\boldsymbol{M}_{k,i}]=\boldsymbol{\mu}_{k,i}, \mathbb{E}[(\boldsymbol{M}_{k,i}-\boldsymbol{\mu}_{k,i})(\boldsymbol{M}_{k,i}-\boldsymbol{\mu}_{k,i})^{\mathrm{T}}]=\boldsymbol{\sigma}_{k,i}\boldsymbol{\sigma}_{k,i}^{\mathrm{T}}\} \tag{27}$$

where $\mathbb{E}[\cdot]$ denotes the expectation operator; $\boldsymbol{\mu}_{k,i}$ is the empirical mean vector of FER i in cluster k; and $\boldsymbol{\sigma}_{k,i}$ is the empirical covariance matrix.

Considering the uncertainty in $\boldsymbol{M}_{k,i}$, the inner approximation method for the DRCC model is simplified as:

$$\inf_{f(\boldsymbol{M}_{k,i})\in\mathcal{D}_i} \Pr\{\boldsymbol{G}_{k,i}\boldsymbol{M}_{k,0}+\boldsymbol{W}_{k,i}\boldsymbol{b}_{k,i}\leq\boldsymbol{M}_{k,i}\}\geq 1-\varepsilon \quad \forall i\in\mathcal{N}_k \tag{28}$$

where ε is the allowable violation probability; and $f(\boldsymbol{M}_{k,i})$ is the probability distribution function of $\boldsymbol{M}_{k,i}$.

The optimal affine transformation parameters $(\boldsymbol{\gamma}_k, \boldsymbol{\varphi}_k, \boldsymbol{G}_{k,i})$ are obtained by solving the following DRCC model, which reformulates (26)-(28) into a tractable linear programming problem to ensure robustness under uncertainty:

$$\begin{cases} \max\limits_{\boldsymbol{\gamma}_k,\boldsymbol{\varphi}_k,\boldsymbol{A}_{k,i},\boldsymbol{b}_{k,i},\boldsymbol{G}_k} Tr(\boldsymbol{\gamma}_k) \\ \text{s.t. } \boldsymbol{\gamma}_{k,i}>0 \quad \forall i\in\mathcal{N}_k \\ \quad \boldsymbol{G}_{k,i}\geq 0 \quad \forall i\in\mathcal{N}_k \\ \quad \boldsymbol{\gamma}_k=\sum\limits_{i\in\mathcal{N}_k}\boldsymbol{A}_{k,i} \\ \quad \boldsymbol{\varphi}_k=\sum\limits_{i\in\mathcal{N}_k}\boldsymbol{b}_{k,i} \\ \quad \boldsymbol{G}_{k,i}\boldsymbol{W}_{k,i}=\boldsymbol{W}_{k,i}\boldsymbol{A}_{k,i} \quad \forall i\in\mathcal{N}_k \\ \quad \boldsymbol{G}_{k,i}(m,:)\boldsymbol{M}_{k,0}+\boldsymbol{W}_{k,i}(m,:)\boldsymbol{b}_{k,i}\leq\boldsymbol{M}_{k,i}(m) \quad m\in Mc \\ \quad \boldsymbol{G}_{k,i}(m,:)\boldsymbol{M}_{k,0}+\boldsymbol{W}_{k,i}(m,:)\boldsymbol{b}_{k,i}\leq\boldsymbol{\mu}_{k,i}(m)-\boldsymbol{\sigma}_{k,i}(m)\sqrt{\dfrac{1-\varepsilon_m}{\varepsilon_m}} \\ \qquad\qquad m\in Mu \end{cases} \tag{29}$$

where m is the row index; Mc and Mu are the sets of rows in $\boldsymbol{M}_{k,0}$ with certain and uncertain parameters, respectively; and ε_m is the violation probability of the m^{th} constraint.

IV. Proposed Coordinated Operation Model for Flexibility Improvement

This section presents the proposed coordinated operation model for improving the flexibility of ADNs. This model integrates the proposed method within an intraday rolling mechanism to dynamically manage heterogeneous user-side FERs including ESs, EVs, and TCLs, as shown in Fig. 2.

A. Quantification of Flexibility Demand of ADNs

Quantifying system flexibility is the initial step in improving the flexibility of ADNs. This quantification enables more effective mitigation of net load fluctuations, improved consumption of distributed renewable generation, and reduced operation costs for the transmission system [29]. A significant mismatch between renewable generation and load demand profiles necessitates additional FERs for balancing. Conversely, a high correlation between renewable generation and demand reduces the need for regulation [30]. This paper introduces a similarity index R to quantitatively assess the correlation between the renewable generation profile and load demand profile, as defined in (30).

$$R(P_{N,t},P_{L,t})=\frac{cov(P_{N,t},P_{L,t})}{\sqrt{\sigma^2_{P_{N,t}}\sigma^2_{P_{L,t}}}} \tag{30}$$

where $cov(P_{N,t},P_{L,t})$ is the covariance between renewable generation $P_{N,t}$ and load demand $P_{L,t}$; and $\sigma^2_{P_{N,t}}$ and $\sigma^2_{P_{L,t}}$ are the variances of $P_{N,t}$ and $P_{L,t}$, respectively. The value range of R is $[-1, 1]$, and the closer it is to 1, the higher the correlation. In this study, a value of $R=1$ is adopted.

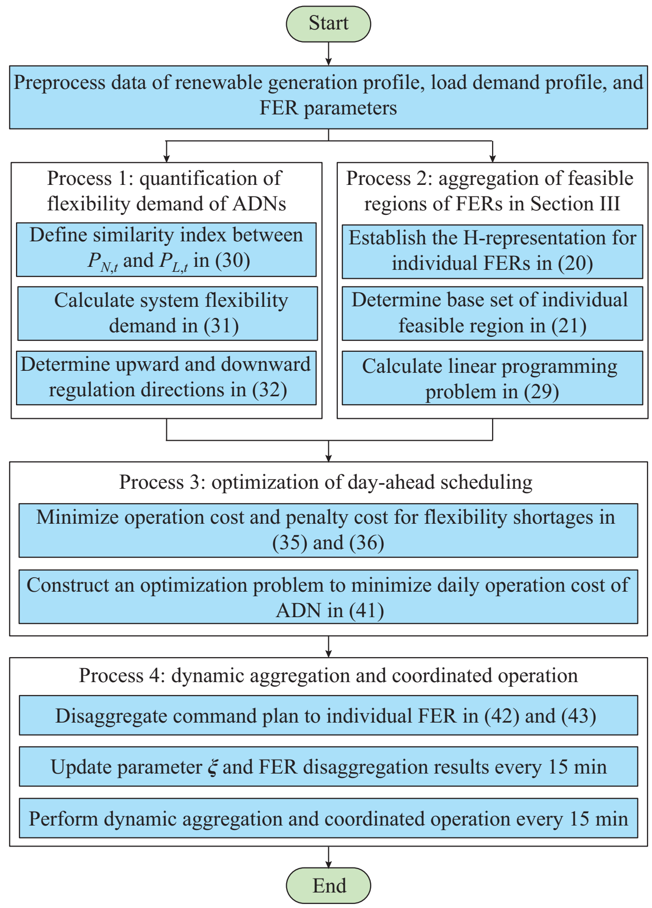

Fig. 2. Diagram of implementation processes of proposed model.

To quantify the system flexibility demand, an ideal renewable generation profile $P^{ideal}_{N,t}$ is formulated to maximize the similarity index R with $P_{L,t}$. This profile ensures optimal synchronization between $P_{N,t}$ and $P_{L,t}$, thereby minimizing the need for flexibility regulation and its associated costs. The flexibility demand P^{flex}_t is defined as the deviation between $P^{ideal}_{N,t}$ and $P_{N,t}$, which represents the regulation requirement to be supplied by FERs. The decision variables $P^{ideal}_{N,t}$ and P^{flex}_t are determined by solving an optimization problem.

$$\begin{cases} \min \sum\limits_{t=1}^{T}|P^{flex}_t| \\ \text{s.t. } R(P^{ideal}_{N,t},P_{L,t})=1 \\ \quad \sum\limits_{t=1}^{T}P_{N,t}=\sum\limits_{t=1}^{T}P^{ideal}_{N,t} \\ \quad P^{flex}_t=P^{ideal}_{N,t}-P_{N,t} \end{cases} \tag{31}$$

where $R(P_{N,t}^{ideal}, P_{L,t})$ is the similarity index with $P_{N,t}^{ideal}$ and $P_{L,t}$.

The regulation direction of flexibility is as follows:

$$\partial_t = \begin{cases} 1 & P_{N,t} > P_{N,t}^{ideal} \\ 0 & P_{N,t} < P_{N,t}^{ideal} \end{cases} \tag{32}$$

where ∂_t is the regulation direction of flexibility at time t. $\partial_t = 1$ indicates downward regulation direction, while $\partial_t = 0$ indicates upward regulation direction.

The flexibility margin, defined as the difference between flexibility supply and demand, quantifies the balance between flexibility supply and demand in the ADN. When flexibility demand exceeds supply, flexibility shortages arise. The upward and downward flexibility shortages are defined as:

$$F_{def,t}^{up} = \begin{cases} \left| F_{VAC,t}^{up} \right| & F_{VAC,t}^{up} \le 0 \\ 0 & F_{VAC,t}^{up} > 0 \end{cases} \tag{33}$$

$$F_{def,t}^{down} = \begin{cases} \left| F_{VAC,t}^{down} \right| & F_{VAC,t}^{down} \le 0 \\ 0 & F_{VAC,t}^{down} > 0 \end{cases} \tag{34}$$

where $F_{VAC,t}^{up}$ and $F_{VAC,t}^{down}$ are the upward and downward flexibility margins, respectively, with non-negative values indicating sufficient flexibility; and $F_{def,t}^{up}$ and $F_{def,t}^{down}$ are the upward and downward flexibility shortages, respectively.

B. Optimization of Day-ahead Scheduling

A day-ahead scheduling model is developed to improve the flexibility of ADNs. To quantify and mitigate flexibility shortages, this model incorporates a penalty cost for flexibility shortages, as imposed by upper-level system operators. Consequently, the objective is to minimize the total operation cost by optimally scheduling various FERs, thereby avoiding such penalties.

1) Operation cost F_1

F_1 comprises the costs of purchasing electricity from the transmission system C_g, the operation cost of renewable generation C_N, the revenue from supplying load C_L, and the operation and compensation cost for FERs C_{FERs}. The sale of electricity from the ADN to the transmission system is excluded from this study.

$$F_1 = \sum_{t=1}^{T} (C_g + C_N - C_L + C_{FERs}) \Delta t \tag{35}$$

2) Penalty cost for flexibility shortage F_2

A penalty cost is introduced to account for flexibility shortages. This penalty cost, denoted as F_2, is defined as:

$$F_2 = \sum_{t=1}^{T} (K_{VAC}^{up} F_{def,t}^{up} + K_{VAC}^{down} F_{def,t}^{down}) \Delta t \tag{36}$$

where K_{VAC}^{up} and K_{VAC}^{diwn} are the unit penalty cost coefficients for insufficient upward and downward flexibility regulation capability, respectively.

3) Optimization model

The objective is to minimize the total cost, which includes F_1 and F_2. The constraints include the FER operation models and aggregated feasible region from Sections II and III, the flexibility regulation direction defined in Section IV, along with the following operational constraints [31]:

$$P_{g,t} + \sum_{i \in \mathcal{N}_k} (P_{FER,i,t}^{D} - P_{FER,i,t}^{C}) - P_{L,t} + P_{N,t} = 0 \tag{37}$$

$$0 \le P_{FER,k,i,t}^{C} \le P_{FER,k,i,t}^{C,\max} \tag{38}$$

$$0 \le P_{FER,k,i,t}^{D} \le P_{FER,k,i,t}^{D,\max} \tag{39}$$

$$0 \le P_{g,t} \le P_{g,t}^{\max} \tag{40}$$

where $P_{g,t}^{\max}$ is the maximum allowable power exchange with the transmission system; $P_{g,t}$ is the power imported from the transmission system at time t; $P_{FER,i,t}^{C}$ and $P_{FER,i,t}^{D}$ are the charging and discharging power of FER i at time t, respectively; $P_{FER,k,i,t}^{C}$ and $P_{FER,k,i,t}^{D}$ are the charging and discharging power of FER i in cluster k at time t obtained from the aggregated feasible region, respectively; and $P_{FER,k,i,t}^{C,\max}$ and $P_{FER,k,i,t}^{D,\max}$ are the maximum values of $P_{FER,k,i,t}^{C}$ and $P_{FER,k,i,t}^{D}$, respectively. Formulas (37)-(40) represent the power balance, the charging power constraint of FERs, the discharging power constraint of FERs, and the grid interaction constraints, respectively.

Integrating (37)-(40), the day-ahead scheduling problem is formulated as the following nonlinear mixed-integer program:

$$\begin{cases} \min F(\boldsymbol{X}) = F_1 + F_2 \\ \text{s.t. (1)-(7), (9)-(14), (16)-(18), (20), (32)-(34), (37)-(40)} \\ \boldsymbol{X} = [P_{g,t}, P_{N,t}, P_{ES,t}^{ch}, P_{ES,t}^{dis}, P_{EV,i,t}^{ch}, P_{EV,i,t}^{dis}, P_{TCL,i,t}] \end{cases} \tag{41}$$

where $\boldsymbol{X}$ denotes the vector of decision variables for power output of various units over the scheduling horizon; and F is the total operating cost. If $F < 0$, the DSO is in a profitable state; otherwise, it is in a loss state.

C. Dynamic Aggregation and Coordinated Operation

This subsection outlines the model for improving flexibility through the dynamic aggregation and coordinated operation of FERs. During actual operation of ADNs, the parameters of FERs are time-varying; therefore, their aggregated feasible region must be updated in real time to capture the flexibility regulation capability. The flexibility regulation capability depends both on these state parameters and the scheduling commands issued by the DSO. Therefore, an aggregator (as a functional module) updates the aggregated feasible region in a rolling manner, thereby forming a dynamic aggregation module that adjusts the scheduling to meet real-time needs of ADNs. The structure of the dynamic aggregation and coordinated operation is illustrated in Fig. 3.

This structure involves three key entities: the DSO, aggregators (including aggregation and disaggregation functions), and FERs. The dynamic aggregation module aims to achieve effective management and control of large-scale, dispersed, and heterogeneous user-side FERs. A 15-min intraday rolling mechanism is adopted to update the uncertain parameters, following the specific steps below.

Step 1: calculate the flexibility capability. Based on the parameters of FERs at $t=1$, the aggregated feasible region is computed using the proposed method.

Step 2: report flexibility capability and receive scheduling command. The dynamic aggregation module reports the aggregated feasible region to the DSO. Considering the flexibility demands of ADNs at $t=1$, the DSO issues scheduling commands. The dynamic aggregation module then performs disaggregation to allocate setpoints to individual FERs, adjusting their operation strategies to meet flexibility demands.

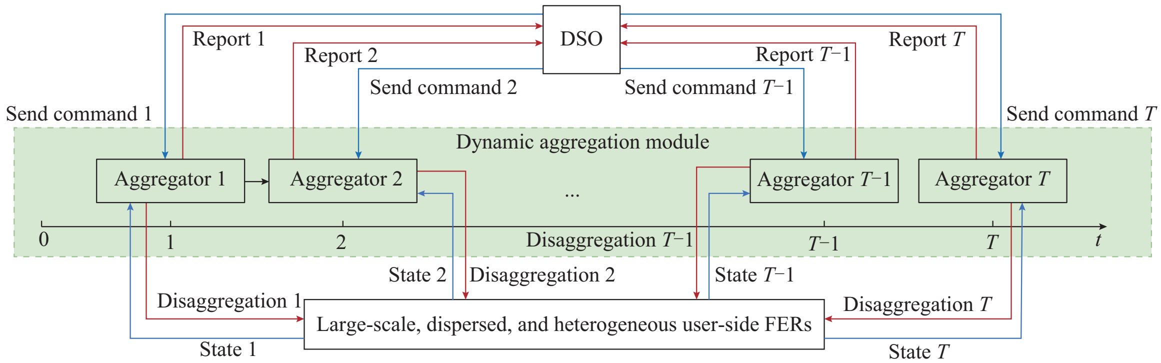

Fig. 3. Structure of dynamic aggregation and coordinated operation.

Step 3: update status parameters and recalculate for next interval. After disaggregation and scheduling, the parameters of FERs are updated at $t=2$. The aggregated feasible region at $t=2$ is then recalculated accordingly.

Step 4: complete dynamic aggregation and coordinated operation cycle. *Steps 1-3* are repeated until $t=T$.

After receiving scheduling commands from the DSO, the disaggregation process allocates setpoints to individual ES, EV, and TCL. The process responds in parallel to the economic scheduling results. The proposed method ensures that the scheduling trajectory of DSO from (41) lies within the aggregated feasible region, enabling each FER to execute its command without additional optimization [25]. Specifically, $A_{FER,k,i,t}$ and $b_{FER,k,i,t}$ are the scaling coefficient and translation offset of FER i in cluster k at time t, respectively. $\gamma_{FER,k,t}$ and $\varphi_{FER,k,t}$ are the base scaling coefficient and base translation offset of cluster k at time t, respectively. The proposed method accounts for both heterogeneity of FERs and temporal variations in their linear transformation matrices. Based on the solution to (29), the disaggregation is performed as:

$$P^{ch}_{FER,k,i,t}=\frac{F^{up}_{FER,i,t}}{F^{up}_{t}}A_{FER,k,i,t}\gamma^{-1}_{FER,k,t}(P^{C}_{FER,k,i,t}-\varphi_{FER,k,t})+b_{FER,k,i,t} \tag{42}$$

$$P^{dis}_{FER,k,i,t}=\frac{F^{down}_{FER,i,t}}{F^{down}_{t}}A_{FER,k,i,t}\gamma^{-1}_{FER,k,t}(P^{D}_{FER,k,i,t}-\varphi_{FER,k,t})+b_{FER,k,i,t} \tag{43}$$

where $P^{C}_{FER,k,i,t}$ and $P^{D}_{FER,k,i,t}$ are the aggregated upward and downward scheduling signals from the DSO, respectively; $P^{ch}_{FER,k,i,t}$ and $P^{dis}_{FER,k,i,t}$ are the upward and downward scheduling signals for FER i in cluster k at time t , respectively; F^{up}_{t} and F^{down}_{t} are the total upward and downward flexibility capabilities at time t, respectively; and $F^{up}_{FER,i,t}$ and $F^{down}_{FER,i,t}$ are the upward and downward capabilities of FER i at time t, respectively.

V. Case Study

In this section, a specific ADN located in Northwest China is used to validate the effectiveness of the proposed method. The voltage level in the ADN is 10 kV, with a maximum base load of 40 MW. The ADN comprises various DERs, namely WGs and PV cells, as well as 108 ESs, 2000 EVs, and 2000 TCLs. With a time step of 15 min, one day is divided into $T=96$ time intervals. All calculations were performed on a desktop computer running the Windows 10 operating system, equipped with an Intel Core i7-14700KF 3.40 GHz CPU and 32.0 GB RAM. The solutions were obtained using MATLAB R2023a, GUROBI 12.0, and MOSEK 10.2 solvers.

A. Flexibility Demand Quantification of Test System

The parameters for EVs and TCLs are assumed to follow specified probability distributions, namely the normal distribution $N(\cdot)$ and the uniform distribution $U(\cdot)$. EVs are divided into three clusters based on $E_{EV,k,i,ta}$ and $E^{e}_{EV,k,i}$, while TCLs are divided into two clusters based on Υ_{set}. The parameters of EV and TCL clusters used in this study are detailed in Tables I and II. Based on the day-ahead forecast output power of WG, PV, and load demand, using the flexibility demand quantification method for ADN with $R=1$ described in Section IV-A, the results of quantifying flexibility demand are presented in Fig. 4.

TABLE I
Parameters of EV Clusters

Parameter	EV cluster 1	EV cluster 2	EV cluster 3
N_{EV}	800	400	800
$t_{EV,k,i,a}$	$N(18,1)$	$N(21,1)$	$N(8,1)$
$t_{EV,k,i,l}$	$N(8,1)$	$N(7,1)$	$N(19,1)$
$E_{EV,k,i,ta}$ (kWh)	$N(16,3^2;0,32)$	$N(22,4^2;0,43)$	$N(18,3^2;0,36)$
$E^{e}_{EV,k,i}$ (kWh)	$N(28,2^2;0,32)$	$N(39,2^2;35,43)$	$N(32,2^2;28,36)$
$P^{\max}_{EV,k,i}$ (kW)	$U(4,7)$	$U(9,12)$	$U(5,8)$
$P^{\min}_{EV,k,i}$ (kW)	$U(-7,-4)$	$U(-12,-9)$	$U(-8,-5)$
$E^{\max}_{EV,k,i}$ (kWh)	32	43	36

As shown in Fig. 4, the shaded areas represent the upward or downward flexibility demand from FERs. Specifically, from 10:00 to 15:00, with an increase in renewable generation, the similarity between renewable generation and load decreases, leading to higher downward flexibility demand.

From 17:00 to 22:00, during the evening peak, the load increases, whereas renewable generation decreases. Since the trends of renewable generation and load are opposite, the highest flexibility demand occurs during this period, requiring more upward flexibility regulation from FERs. The proposed method successfully captures these temporal variations in flexibility demand, providing a basis for scheduling and FER allocation.

TABLE II
PARAMETERS OF TCL CLUSTERS

Parameters	TCL cluster 1	TCL cluster 2
N_{TCL}	800	1200
$P_{TCL,k,i}^{\max}$ (kW)	$U(3,7)$	$U(3,6)$
$P_{TCL,k,i}^{\min}$ (kW)	0	0
Capacitance (kWh/℃)	$U(2,3)$	$U(2,3)$
Resistance (℃/kW)	$U(2,3)$	$U(2,3)$
Υ_{set} (℃)	$N(19,2^2;16,22)$	$N(24,2^2;23,27)$

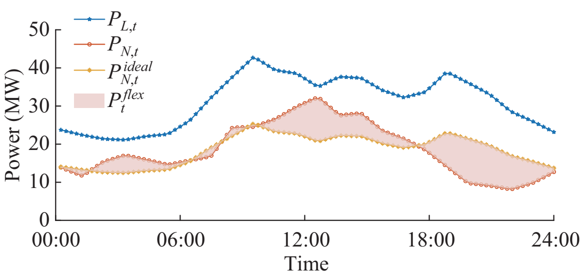

Fig. 4. Results of quantifying flexibility demand.

B. Comparison of Aggregation Methods

This subsection validates the effectiveness of the proposed method for EVs and TCLs. As illustrated in Section III, this study analyzes the effects of different uncertainty levels and violation probabilities ε in the chance constraints of (28) on the aggregated feasible region. Using TCLs as an example, we vary ε from 0.01 to 0.15 and set the ambient temperature uncertainty levels to 0.03. Figure 5 shows that as the violation probability decreases, the confidence level in the estimated parameters for the feasible region increases, resulting in a more conservative aggregated feasible region.

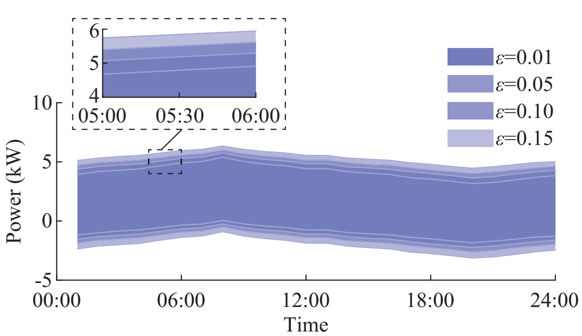

Fig. 5. Feasible regions under different violation probabilities.

The performance of the proposed method was compared with that of the traditional polytope-based aggregation methods in [11] based on inner approximation and outer approximation (OA), which are denoted as method 1 and method 2. The violation probability ε for both $E_{EV,k,i,ta}$ and Υ_{out} is set to be 0.05. In Fig. 6, three TCLs of type TCL2 (TCL21, TCL22, and TCL23) are used as a small-scale example to present the exact region for each TCL, as well as the feasible regions obtained by method 1 and proposed method, which can be simplified for intuitive visualization and clear explanation. Figure 7 considers 100 TCLs as a large-scale example to present the comparison of feasible regions obtained by different methods.

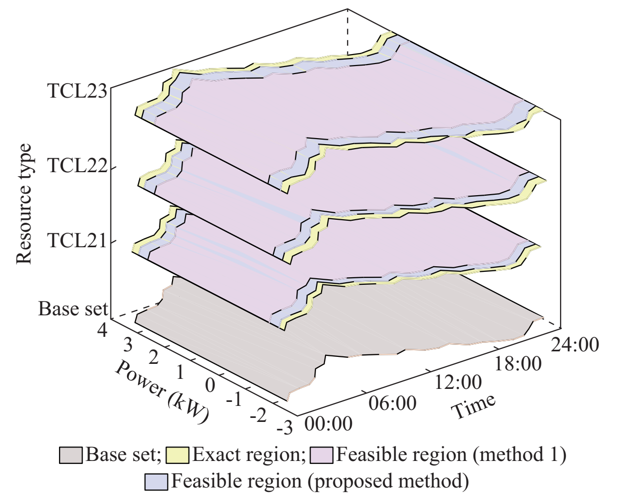

Fig. 6. Exact region and feasible regions obtained by method 1 and proposed method.

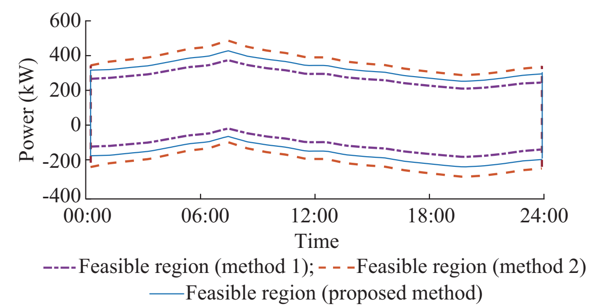

Fig. 7. Comparison of feasible regions obtained by different methods.

In Fig. 6, the base sets of three TCLs are obtained according to (21). For each TCL, the area of the exact region is larger than that of the feasible regions obtained by method 1 and proposed method. Furthermore, compared with the feasible region obtained by method 1, the feasible region obtained by the proposed method is closer to the exact region. Therefore, the proposed method reduces the conservatism of method 1 at the single-FER level.

In Fig. 7, the feasible region obtained by method 2 overestimates the exact region and leads to infeasibility during disaggregation. In contrast, the feasible region obtained by method 1 can preserve the structure of the base set and avoid infeasible solutions. However, method 1 sacrifices part of the feasible region of FERs and does not fully account for the diversity and heterogeneity of individual FERs at different time, thus underestimating the flexibility capability bound and potentially wasting their flexibility regulation capability during system operation. The feasible region obtained by the proposed method lies between those of methods 1 and 2. The proposed method can more accurately capture the feasible region of FERs compared with existing methods.

In method 1, the transformation matrix γ_k is simplified to a scalar, representing only a single scale factor. This simplification neglects the effects of other potential linear transformations such as rotation and shear. In contrast, the affine transformation matrix γ_k utilized in this study represents a full-dimensional linear transformation, capturing a broader range of transformations including rotation, scaling, and shear. To further evaluate the accuracy of the proposed method, the 2-norm of the $2T\times 2T$ transformation matrix $\|\gamma_k\|_2$ is calculated, which reflects the maximum scaling factor. Table III presents the comparison of the proposed method and method 1 based on the results of five independent tests.

TABLE III
COMPARISON OF DIFFERENT METHODS BASED ON RESULTS OF FIVE INDEPENDENT TESTS

Method	Average scaling factor	Average solution time (s)
Method 1	7.559	0.947
Proposed method	8.036	0.981

As shown in Table III, the proposed method has a slightly longer solution time than method 1 due to its affine transformation structure. However, this additional time—within 0.05 s (3.5% of the total solution time)—is a justifiable trade-off for higher aggregation accuracy and does not significantly affect the scheduling decision process. Overall, the proposed method achieves better accuracy and delivers more robust and adaptable responses to dynamic changes.

To further evaluate computational performance and scalability, we analyzed the solution time against the number of EVs (N_{EV}) for the proposed method and three existing aggregation methods: the analytical polytope approximation (APA) [32], the homothet-based method (HM) [11], and the structure-preserving transformation (SPT) [17]. Figure 8 shows the impact of N_{EV} on the solution time and flexibility loss.

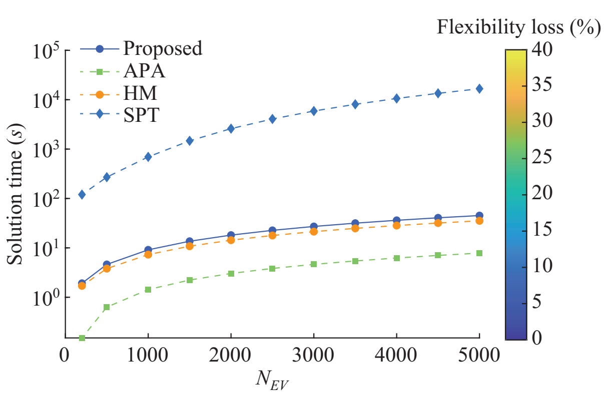

Fig. 8. Impact of N_{EV} on solution time and flexibility loss.

As shown in Fig. 8, while the SPT achieves high accuracy (10% flexibility loss), it exhibits a steep and super-linear increase in solution time with N_{EV}, rendering it impractical for large-scale applications. In contrast, APA maintains low solution time at the expense of higher flexibility loss (27%). The proposed method demonstrates a manageable growth in solution time comparable to HM, yet achieves this with the highest accuracy (6% flexibility loss). This favorable scalability stems from its decomposable structure, which enables parallel solving of N_{EV} independent sub-problems. Consequently, while not the absolute fastest, the proposed method maintains the lowest flexibility loss across all tested scales within practically acceptable time frames. This effective trade-off establishes the proposed method as a highly competitive solution for flexibility aggregation.

C. Aggregated Feasible Regions of EV and TCL Clusters

This subsection analyzes the aggregated feasible regions of different clusters. Figure 9 shows the aggregated feasible regions of EV and TCL clusters, where $\bar{P}_{EV,k}$ and $\underline{P}_{EV,k}$ are the upper and lower power bounds of EV of cluster k, respectively; and $\bar{P}_{TCL,k}$ and $\underline{P}_{TCL,k}$ are the upper and lower power bounds of TCL of cluster k, respectively.

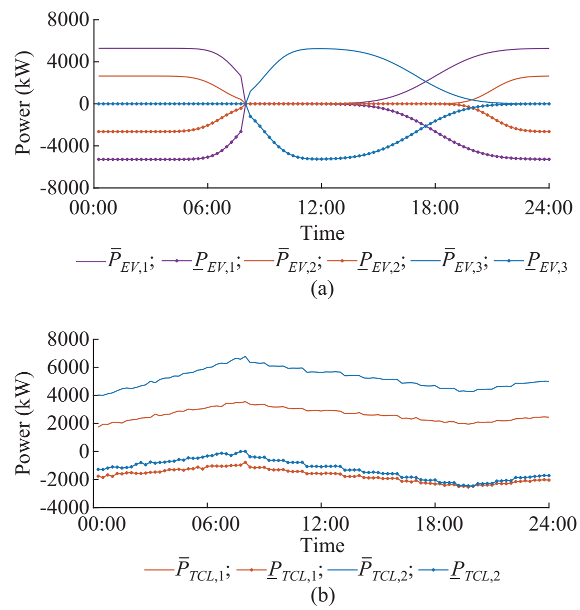

Fig. 9. Aggregated feasible regions of EV and TCL clusters. (a) Aggregated feasible region of EV clusters. (b) Aggregated feasible region of TCL clusters.

Figure 9(a) shows the aggregated feasible regions of different EV clusters. Variations in individual parking characteristics and initial charging state lead to differences in the power bounds across the clusters. These differences indicate that each EV cluster has different flexibility regulation capability, enabling effective regulation to be achieved across 96 time intervals in a day. Figure 9(b) shows the aggregated feasible regions of different TCL clusters. To analyze the charging and discharging characteristics of TCLs, their behavior is characterized by the difference between the actual power demand and the reference power. Negative values denote time intervals where actual power is below the reference power. The aggregated feasible regions exhibit an inverse relationship with ambient temperature. Specifically, TCL1 and

TCL2 exhibit similar downward flexibility regulation capacities. However, the downward flexibility capability of TCL2 is lower than that of TCL1 due to its higher temperature setpoint, despite having more units. Thus, TCL2 demonstrates a lower downward regulation capability but a higher upward regulation capability.

D. Day-ahead Scheduling Results with Proposed Coordinated Operation Model

To evaluate the accuracy and efficiency of the proposed method, a comparative analysis of several scenarios is performed, as detailed in Table IV. Table V presents the results of the four scenarios. Since the tractable linear programming problem (29) for each ES, EV, and TCL can be solved in parallel, the overall solution time of the proposed method mainly depends on solving (29) and the day-ahead scheduling model (41). Figure 10 illustrates the flexibility regulation capabilities of the proposed method in Scenario 4 in day-ahead scheduling, where up and down denote the upward and downward regulation capability, respectively.

TABLE IV
COMPARATIVE ANALYSIS OF FOUR SCENARIOS

Scenario	Aggregation	Clustering	Flexibility	Economic
1	×	×	√	√
2	√	×	√	√
3	√	√	√	×
4	√	√	√	√

Note: √ and × denote the presence and absence of each feature in the scenario, respectively.

TABLE V
RESULTS OF DIFFERENT SCENARIOS

Comparison term	Scenario 1	Scenario 2	Scenario 3	Scenario 4
Purchasing electricity cost (¥)	276283	275862	278123	276154
Renewable generation cost (¥)	342118	342118	342118	342118
Compensation cost (¥)	85854	86132	155952	85833
Penalty cost (¥)	3431	4220	0	3649
Revenue (¥)	−725232	−725032	−756138	−725153
Total cost (¥)	−17544	−16698	20055	−17396
Peak-valley difference of net load (kW)	8783.01	9397.52	8783.01	8783.01
Similarity index	0.9918	0.9850	1.0000	0.9998
Solution time (s)	2220.17	21.96	21.98	21.98

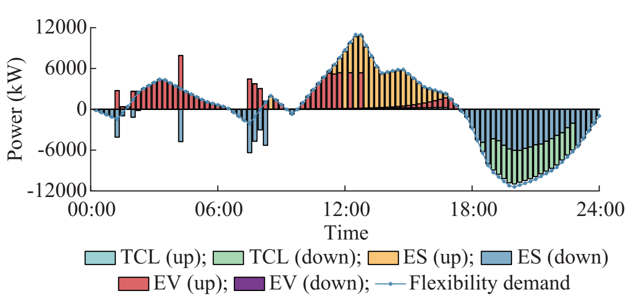

Fig. 10. Flexibility regulation capabilities of proposed method in Scenario 4 in day-ahead scheduling.

In Table V, Scenario 1 achieves the lowest total cost, corresponding to the highest revenue, as it fully exploits the flexibility regulation capability of FERs and incurs a lower penalty for flexibility shortages. However, its long solution time resulting from modeling each FER individually makes it impractical for large-scale scheduling. Scenario 3 achieves the highest source-load similarity, thereby significantly improving the flexibility of ADNs and avoiding penalties for flexibility shortages, but at the expense of highest compensation cost (¥155952) due to extensive use of FERs. Scenarios 2 and 4 have similar total costs. However, Scenario 2 performs aggregation without clustering, increasing the peak-valley difference of net load and the penalty cost by 614.51 kW and ¥571, respectively. Compared with Scenario 1, Scenario 4 reduces the solution time from 2220.17 s to just 21.98 s, while maintaining the same peak-valley difference of net load as Scenarios 1 and 3, at 8783.01 kW. Overall, the proposed method in Scenario 4 avoids a heavy computational burden while preserving optimization effectiveness.

As shown in Fig. 10, each FER provides different levels of upward and downward flexibility regulation capability. Considering the constraints of the charging/discharging power and state of charge, when the downward flexibility regulation capability exceeds the demand, ESs and TCLs work together to balance the actual flexibility regulation. However, from 18:00 to 22:00, upward flexibility capability is insufficient due to evening peak demand exceeding the flexibility regulation capability of FERs. Therefore, the DSO must purchase power from the transmission system. EVs primarily provide downward flexibility regulation capability, as their discharge compensation cost is higher than that of TCLs. In contrast, TCLs have greater upward flexibility regulation capability and can collaborate with EVs to provide joint flexibility regulation services. From 12:00 to 17:00, TCLs also contribute downward flexibility regulation capability. During this period of peak ambient temperature, users typically maintain the relatively low temperature setpoints, enabling TCLs to offer downward flexibility regulation capability and alleviate pressure on the ADN. In summary, integrating complementary FER clusters effectively expands the system-level aggregated feasible region.

A comprehensive performance comparison is conducted against three existing aggregation methods: APA [32], SPT [17], and method 2. The results, summarized in Table VI, demonstrate the superior overall performance of the proposed method in balancing flexibility, feasibility, and efficiency. Although method 2 is computationally fastest and achieves the lowest total cost, its infeasibility rate of 21% compromises practical applicability. In contrast, APA and SPT guarantee feasibility but exhibit distinct trade-offs: APA suffers from high flexibility loss (27.0%) due to its use of constant scaling factors, while SPT achieves higher accuracy but requires significantly longer solution time (1042.60 s) due to coupled constraints. The proposed method effectively reconciles these trade-offs by using linear transformation matrices, achieving flexibility (6% flexibility loss) and solution time (21.98 s) within a tractable linear programming problem.

TABLE VI
PERFORMANCE COMPARISON OF DIFFERENT METHODS

Comparison term	APA	SPT	OA	Proposed
Feasibility loss (%)	27	10	0	6
Total cost (¥)	–14084	–15223	–20249	–17396
Peak-valley difference of net load (kW)	9415.27	10086.00	8815.50	8783.01
Similarity index	0.8652	0.9907	1.0000	0.9998
Infeasibility rate (%)	0	0	21	0
Solution time (s)	13.10	1042.60	0.74	21.98

E. Intraday Dynamic Aggregation and Scheduling of FERs

This subsection evaluates the proposed intraday rolling mechanism through a 15-min rolling window simulation based on intraday renewable generation, load, and temperature data. We propose a coordinated day-ahead and intraday scheduling model that quantifies the real-time regulation capability of EVs and TCLs by analyzing their state changes from observational data, enabling rolling updates and corrections to the aggregated feasible region. The day-ahead and intraday rolling scheduling results for different FER clusters are shown in Fig. 11, where $P^{up}_{EV,2,plan,t}$ and $P^{down}_{EV,2,plan,t}$ are the day-ahead upward and downward regulation power of EV cluster 2, respectively; $P^{up}_{EV,2,real,t}$ and $P^{down}_{EV,2,real,t}$ are the intraday real-time upward and downward regulation power of EV cluster 2, respectively; $P^{up}_{TCL,2,plan,t}$ and $P^{down}_{TCL,2,plan,t}$ are the day-ahead upward and downward regulation power of TCL cluster 2, respectively; and $P^{up}_{TCL,2,real,t}$ and $P^{down}_{TCL,2,real,t}$ are the intraday real-time upward and downward regulation power of TCL cluster 2, respectively.

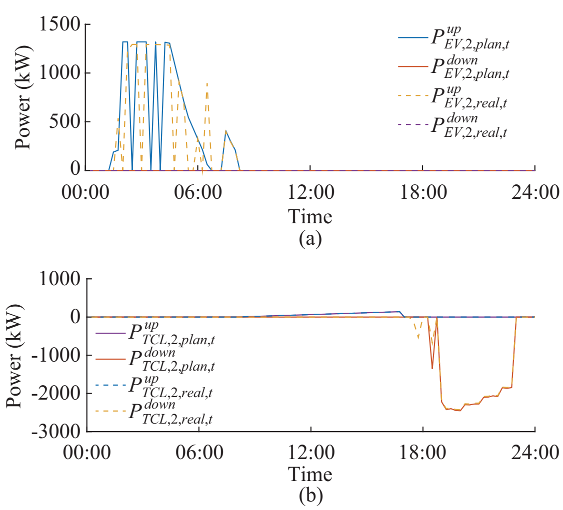

Fig. 11. Day-ahead and intraday rolling scheduling results for different FER clusters. (a) EV cluster. (b) TCL cluster.

The results in Fig. 11 demonstrate that EVs are used for downward flexibility regulation, whereas upward flexibility regulation is handled by TCLs. This coordinated day-ahead and intraday scheduling model enables optimized resource utilization across different FER clusters to meet system flexibility demands. Within the constraints of the dynamically aggregated feasible regions, the intraday rolling mechanism continuously adjusts the intraday rolling scheduling. Although the intraday rolling scheduling deviates from the day-ahead rolling scheduling, the day-ahead rolling scheduling correctly identifies the timing and direction for flexibility regulation, offering a reliable reference for real-time operations.

VI. CONCLUSION

This paper proposes a polytope-based aggregation method for user-side FERs using affine transformation to improve the flexibility of ADNs. A coordinated operation model applying the proposed method is established to enhance the economic performance and operational efficiency of modern distribution networks. Test cases validate that, compared to the traditional inner approximation methods, the proposed method effectively captures the heterogeneity of individual FERs, reducing the conservatism of the aggregated feasible region and achieving higher optimization accuracy. Furthermore, it significantly reduces the computational burden for both day-ahead and intraday rolling scheduling, enhancing overall system flexibility without compromising economic benefits.

Future research will explore uncertainties from renewable generation and load on FER aggregation, along with user behavior and state dynamics, which aims to extend the proposed method for enhanced operational feasibility under more complex real-world conditions.

REFERENCES

[1] Y. Zhao, G. Zhang, W. Hu *et al.*, “Meta-learning based voltage control for renewable energy integrated active distribution network against topology change,” *IEEE Transactions on Power Systems*, vol. 38, no. 6, pp. 5937-5940, Nov. 2023.

[2] G. Song, C. Ma, H. Ji *et al.*, “Bi-level supply restoration method for active distribution networks considering multi-resource coordination,” *Journal of Modern Power Systems and Clean Energy*, vol. 13, no. 3, pp. 967-979, May 2025.

[3] M. Yang, Y. Wang, J. Wang *et al.*, “Optimal scheduling of integrated energy systems in low-carbon communities considering flexibility of resources and segmental control of solid oxide fuel cells,” *Journal of Modern Power Systems and Clean Energy*, vol. 13, no. 3, pp. 915-927, May 2025.

[4] G. Tsaousoglou, I. Sartzetakis, P. Makris *et al.*, “Flexibility aggregation of temporally coupled resources in real-time balancing markets using machine learning,” *IEEE Transactions on Industrial Informatics*, vol. 18, no. 7, pp. 4342-4351, Jul. 2022.

[5] A. Churkin, W. Kong, J. N. M. Gutierrez *et al.*, “Tracing, ranking and valuation of aggregated DER flexibility in active distribution networks,” *IEEE Transactions on Smart Grid*, vol. 15, no. 2, pp. 1694-1711, Mar. 2024.

[6] X. Wang, F. Li, J. Dong *et al.*, “Tri-level scheduling model considering residential demand flexibility of aggregated HVACs and EVs under distribution LMP,” *IEEE Transactions on Smart Grid*, vol. 12, no. 5, pp. 3990-4002, Sept. 2021.

[7] Z. Tan, A. Yu, H. Zhong *et al.*, “Optimal virtual battery model for aggregating storage-like resources with network constraints,” *CSEE Journal of Power and Energy Systems*, vol. 10, no. 4, pp. 1843-1847, Jul. 2024.

[8] J. Hu, J. Wu, X. Ai *et al.*, “Coordinated energy management of prosumers in a distribution system considering network congestion,” *IEEE Transactions on Smart Grid*, vol. 12, no. 1, pp. 468-478, Jan. 2021.

[9] S. Zhang, S. Ge, H. Liu *et al.*, “An analytical method for delineating feasible region for PV integration capacities in net-zero distribution systems considering battery energy storage system flexibility,” *Journal of Modern Power Systems and Clean Energy*, vol. 12, no. 2, pp. 475-

487, Mar. 2024.
[10] S. Wang and W. Wu, "Aggregate flexibility of virtual power plants with temporal coupling constraints," *IEEE Transactions on Smart Grid*, vol. 12, no. 6, pp. 5043-5051, Nov. 2021.
[11] L. Zhao, W. Zhang, H. Hao *et al.*, "A geometric approach to aggregate flexibility modeling of thermostatically controlled loads," *IEEE Transactions on Power Systems*, vol. 32, no. 6, pp. 4721-4731, Nov. 2017.
[12] M. P. Evans, S. H. Tindemans, and D. Angeli, "Flexibility framework with recovery guarantees for aggregated energy storage devices," *IEEE Transactions on Smart Grid*, vol. 13, no. 5, pp. 3519-3531, Sept. 2022.
[13] T. Zhang, J. Wang, H. Wang *et al.*, "On the coordination of transmission-distribution grids: a dynamic feasible region method," *IEEE Transactions on Power Systems*, vol. 38, no. 2, pp. 1857-1868, Mar. 2023.
[14] Z. Zheng, J. Li, X. Liu *et al.*, "A de-aggregation strategy based optimal co-scheduling of heterogeneous flexible resources in virtual power plant," *Applied Energy*, vol. 383, p. 125404, Apr. 2025.
[15] Y. Wen, Z. Hu, J. He *et al.*, "Improved inner approximation for aggregating power flexibility in active distribution networks and its applications," *IEEE Transactions on Smart Grid*, vol. 15, no. 4, pp. 3653-3665, Jul. 2024.
[16] M. Zhang, Y. Xu, X. Shi *et al.*, "A fast polytope-based approach for aggregating large-scale electric vehicles in the joint market under uncertainty," *IEEE Transactions on Smart Grid*, vol. 15, no. 1, pp. 701-713, Jan. 2024.
[17] F. A. Taha, T. Vincent, and E. Bitar, "An efficient method for quantifying the aggregate flexibility of plug-in electric vehicle populations," *IEEE Transactions on Smart Grid*, vol. 16, no. 4, pp. 3142-3154, Jul. 2025.
[18] F. L. Muller, J. Szabo, O. Sundstrom *et al.*, "Aggregation and disaggregation of energetic flexibility from distributed energy resources," *IEEE Transactions on Smart Grid*, vol. 10, no. 2, pp. 1205-1214, Mar. 2019.
[19] Z. Yi, Y. Xu, W. Gu *et al.*, "Aggregate operation model for numerous small-capacity distributed energy resources considering uncertainty," *IEEE Transactions on Smart Grid*, vol. 12, no. 5, pp. 4208-4224, Sept. 2021.
[20] Z. Yi, Y. Xu, W. Gu *et al.*, "A multi-time-scale economic scheduling strategy for virtual power plant based on deferrable loads aggregation and disaggregation," *IEEE Transactions on Sustainable Energy*, vol. 11, no. 3, pp. 1332-1346, Jul. 2020.
[21] Q. Wang, C. Huang, C. Wang *et al.*, "Risk-averse frequency regulation strategy of electric vehicle aggregator considering multiple uncertainties," *Applied Energy*, vol. 387, p. 125873, Jun. 2025.
[22] H. Liang, H. Hua, Y. Qin *et al.*, "Stochastic optimal energy storage management for energy routers via compressive sensing," *IEEE Transactions on Industrial Informatics*, vol. 18, no. 4, pp. 2192-2202, Apr. 2022.
[23] H. Zhao, B. Wang, X. Wang *et al.*, "Active dynamic aggregation model for distributed integrated energy system as virtual power plant," *Journal of Modern Power Systems and Clean Energy*, vol. 8, no. 5, pp. 831-840, Sept. 2020.
[24] J. Zhu, Y. Xu, N. Tai *et al.*, "Joint chance-constrained energy-reserve co-optimization for distribution networks with flexible resource aggregators," *Applied Energy*, vol. 388, p. 125685, Jun. 2025.
[25] J. Liu, X. Ai, J. Fang *et al.*, "Continuous-time aggregation of massive flexible HVAC loads considering uncertainty for reserve provision in power system dispatch," *IEEE Transactions on Smart Grid*, vol. 15, no. 5, pp. 4835-4849, Sept. 2024.
[26] W. Zha, H. Zhong, and Y. Liu, "Fair and efficient profit allocation for collaborative operation of distributed renewable energy operators and electric vehicle charging stations," *Journal of Modern Power Systems and Clean Energy*, vol. 13, no. 4, pp. 1395-1406, Jul. 2025.
[27] X. Chen, Y. Lin, Q. Yang *et al.*, "A distributed coordinated control strategy for large-scale thermostatically controlled loads considering user comfort constraints," *Journal of Modern Power Systems and Clean Energy*, vol. 13, no. 3, pp. 1014-1025, Jul. 2025.
[28] P. Cai, C. Wen, B. Cao *et al.*, "A Wasserstein metric distributionally robust chance-constrained peer aggregation energy sharing mechanism for hydrogen-based microgrids considering low-carbon drivers," *Energy*, vol. 325, p. 136178, Jun. 2025.
[29] J. Yang, H. Zhang, C. Li *et al.*, "Quantifying the flexibility regulation potential and economic value of pumped storage in extreme scenarios of multi-energy complementary system," *Energy*, vol. 329, p. 136749, Aug. 2025.
[30] J. Jian, P. Li, H. Ji *et al.*, "DLMP-based quantification and analysis method of operational flexibility in flexible distribution networks," *IEEE Transactions on Sustainable Energy*, vol. 13, no. 4, pp. 2353-2369, Oct. 2022.
[31] Q. Li, F. Dong, G. Zhou *et al.*, "Co-optimization of virtual power plants and distribution grids: emphasizing flexible resource aggregation and battery capacity degradation," *Applied Energy*, vol. 377, p. 124519, Jan. 2025.
[32] J. Jian, M. Zhang, Y. Xu *et al.*, "An analytical polytope approximation aggregation of electric vehicles considering uncertainty for the day-ahead distribution network dispatching," *IEEE Transactions on Sustainable Energy*, vol. 15, no. 1, pp. 160-172, Jan. 2024.

Jing Wang received the M.S. degree in electrical engineering from Xinjiang Agricultural University, Urumqi, China, in 2022. She is currently pursuing the Ph.D. degree in electrical engineering at Xinjiang University, Urumqi, China. Her research interests include electricity market, demand-side management, and distributionally robust optimization in power and energy systems.

Muyang Liu received the M.S. and Ph.D. degrees in electrical energy engineering from University College Dublin, Dublin, Ireland, in 2016 and 2019, respectively. She served as a Senior Researcher at University College Dublin from 2019 to 2020. She is currently a Professor with Xinjiang University, Urumqi, China. Her research focuses on power system modeling and stability analysis.

Junru Chen received the M.S. and Ph.D. degrees in electrical energy engineering from University College Dublin, Dublin, Ireland, in 2016 and 2019, respectively. He was a Senior Researcher at University College Dublin and a Visiting Scholar at Aalborg University, Aalborg, Denmark, in 2020. Since 2020, he has been a Professor at Xinjiang University, Urumqi, China. His current research interests include power electronics control, modeling, stability, and application.

Haochen Hua received the B.Sc. degree in mathematics and finance and the Ph.D. degree in mathematical sciences from the University of Liverpool, Liverpool, U.K., in 2011 and 2016, respectively. From 2016 to 2020, he was a Postdoctoral Fellow with the Research Institute of Information Technology, Tsinghua University, Beijing, China. Since 2020, he has been a Professor with the College of Energy and Electrical Engineering, Hohai University, Nanjing, China. His research interests include energy internet system modeling and optimization, optimal and robust control theory, and stochastic calculus.

Lijiao Gong received the M.S. degree in measuring technology and instruments from Nanjing University of Aeronautics and Astronautics (NUAA), Nanjing, China, in 2008, and the Ph.D. degree in instrumentation science and technology from University of Science and Technology of China (USTC), Hefei, China, in 2015. She is currently a Professor with Shihezi University, Shihezi, China. Her research interests include multiagent cooperative control and its application, and source-grid coordinated control technology for renewable energy source.

Weiqing Wang received the M.S. degree in electrical engineering from the Department of Electrical Engineering, Zhejiang University, Hangzhou, China, in 1990. He is currently a Professor with the Department of Electrical Engineering, Xinjiang University, Urumqi, China. His research interests include development of key components of large-scale wind turbines, intelligent control and detection of whole machine, relay protection, and grid-connected transmission technology.